Direct Real-Time Imaging of Protein Adsorption onto Hydrophilic and Hydrophobic Surfaces

Simon J. Haward,[1] Peter R. Shewry,[2] Mervyn J. Miles,[1] Terence J. Mcmaster[1]

[1] H. H. Wills Physics Laboratory, University of Bristol, Tyndall Avenue, Bristol BS8 1TL, United Kingdom

[2] Rothamsted Research Institute, Harpenden, Herts. AL5 2JQ, United Kingdom

ABSTRACT:

Atomic force microscopy has been used to follow in real time the adsorption from solution of two of the gliadin group of wheat seed storage proteins onto hydrophilic (mica) and hydrophobic (graphite) surfaces. The liquid cell of the microscope was used initially to acquire images of the substrate under a small quantity of pure solvent (1% acetic acid). Continuous imaging as an injection of gliadin solution entered the liquid cell enabled the adsorption process to be followed in situ from zero time. For ω-gliadin, a monolayer was formed on the mica substrate during a period of ∼2000 s, with the protein molecules oriented in parallel to the mica surface. In contrast, the ω-gliadin had a relatively low affinity for the graphite substrate, as demonstrated by slow and weak adsorption to the surface. With γ-gliadin, random deposition onto the mica surface was observed forming monodispersed structures, whereas on the graphite surface, monolayer islands of protein were formed with the protein molecules in a perpendicular orientation. Sequential adsorption experiments indicated strong interactions between the two proteins that, under certain circumstances, caused alterations to the surface morphologies of preadsorbed species. The results are relevant to our understanding of the interactions of proteins within the hydrated protein bodies of wheat grain and how these determine the processing properties of wheat gluten and dough. © 2009 Wiley Periodicals, Inc. Biopolymers 93: 74–84, 2010.

Keywords: Gliadin; AFM; surface adsorption; SPM; tapping mode

INTRODUCTION

Atomic force microscopy (AFM) has been a primary catalyst for intensive research of biomolecules at the single molecule level. Use of an AFM in a liquid environment allows surface-adsorbed molecules to be imaged and/or manipulated in situ in physiological buffer solutions.[1] This also allows the possibility to observe dynamic biological processes on the surface because the imaging environment is altered by, for example, the addition of denaturants or reducing agents to the buffer solution.[2] Alternatively, by imaging a surface in a pure solvent and subsequently injecting a solution of molecules, the adsorption process itself can be followed from zero time.[3–5]

In this study, we describe the use of atomic force microscopy in liquid to compare the real-time, in situ, adsorption from solution of two of the proteins found in wheat gluten, ω- and γ-gliadin, to hydrophilic (mica) and hydrophobic (graphite) surfaces.

AFM has been used successfully in the past to image the adsorption dynamics of C hordein protein of barley to

untreated mica and highly oriented pyrolytic graphite (HOPG) surfaces.[6] This protein is closely related to the ω-gliadins, although it may have a more highly extended chain conformation.[7] The C hordein was dissolved in 0.1 M acetic acid and was imaged in situ in real time as the adsorption process occurred. The results indicated that the protein adsorbed to mica with the long molecular axis parallel to the substrate and that adsorption was favored at the edges of pre-adsorbed structures. Adsorption to the hydrophobic HOPG surface was much more rapid than when hydrophilic mica was used, indicating that protein–protein interactions were the dominant factor in controlling the adsorption behavior in this system. Recently, McIntire et al.[8] have used noncontact AFM to study the conformation of the high-molecular-weight glutenin subunits of wheat adsorbed to hydrophilic and hydrophobic surfaces.

Other examples of protein adsorption studied with AFM include the direct imaging of the adsorption dynamics of immunoglobulin[3] and lysozyme[9] and the observation of plasma protein film formation.[5] In situ AFM methods have also been successfully applied to study the degradation of A-gliadin fibrils[2] and the adsorption and self-assembly of macromolecules.[4]

The ω- and γ-gliadin proteins used in this study are two of a group of wheat seed storage proteins (called gliadins) that are characterized by high proportions of the amino acids proline and glutamine. In wheat dough, they interact with a second group of proteins (called glutenins) to form a viscoelastic mass (gluten). The glutenins form high M_r disulphide stabilized polymers, providing the gluten elasticity, whereas the monomeric gliadins contribute to the viscosity and extensibility of the dough.[10] The gliadins, in particular, are also known to be highly surface active and are likely to play an important role in stabilizing gas bubbles in the dough by adsorption to the gas–liquid interface.[11,12] The formation of a strong viscoelastic gluten network and the stability of entrapped bubbles in the dough are important factors determining the quality of wheat for breadmaking and other end uses. A recent AFM study has used force spectroscopy methods (stretching molecules between the AFM probe and the substrate) to measure the nanomechanical interactions between ω- and α-gliadin proteins.[13] The study suggests that different proteins within the gliadin group may also play different roles in giving wheat dough its unique processing properties.

The ω-gliadins form part of the sulfur-poor group of storage proteins, which also includes the ω-secalins of rye and the C hordeins of barley.[7] They consist almost entirely of repeat motifs (usually based on the octapeptide P-Q-Q-P-F-P-Q-Q) with a M_r of $\sim$40,000.[14] Circular dichroism (CD) spectroscopy of these proteins in solution has indicated a secondary structure consisting of an equilibrium between β-reverse turn and poly-L-proline II-like structure (sometimes referred to as a 'β-spiral'),[15] and this is supported by Fourier transform infrared (FTIR) spectroscopy.[16] However, as the concentration of protein in solution was increased and the hydrated solid state was approached, the secondary structure was observed to change to a mixture of β-reverse turn and intermolecular β-sheet. Scanning tunneling microscopy (STM) and small angle x-ray scattering (SAXS) studies of ω-gliadin have revealed a rod-like structure for the protein with a long axis of $\sim$15 nm and a diameter of $\sim$4 nm.[17]

The γ-gliadins belong to the sulfur-rich group of storage proteins together with the α- and β-gliadins and the low-molecular-weight glutenin subunits of wheat, the γ and B hordeins of barley and the γ-secalins of rye.[7] The γ-gliadins consist of an N-terminal domain comprising heptapeptide repeats related to those in ω-gliadins (consensus P-Q-Q-P-F-P-Q) and a nonrepetitive C-terminal domain, with a M_r of between 30,000 and 45,000. The repetitive sequences are predicted to form β-reverse turns and poly-L-proline II-like structures as in the ω-gliadins, whereas nonrepetitive domains contain four interchain disulphide bonds and are predicted to be globular with a high content of α-helix.[18] STM images of γ-gliadins indicate that these domains form separate structures, with a rod-like repetitive domain of dimensions $\sim$6 × 2.5 nm and a compactly folded nonrepetitive domain of dimensions $\sim$6 × 5 nm. The total length of the molecule is $\sim$12 nm.[19] Reversed phase high-performance liquid chromatography (RP-HPLC) of gliadins has shown that γ-gliadin has a greater surface hydrophobicity than ω-gliadin.[20] Because the repetitive domain of γ-gliadin is very similar to the structure of ω-gliadin, it is expected that nonpolar hydrophobic residues will be concentrated in the nonrepetitive C-terminal domain of the γ-gliadin molecule.

Örnebro et al.[11,12] have studied the adsorption of wheat gliadins to hydrophobic methylated silica surfaces using ellipsometry. They found that adsorption of ω-gliadin was favored with the long axis parallel to the surface, regardless of protein concentration. In the case of γ-gliadin, adsorption occurred parallel to the surface at low protein concentration but became increasingly perpendicular as the concentration was increased, allowing a greater amount of protein to adsorb. Comparison of the adsorption behavior of α- and β-gliadins with that of ω-gliadins led to the suggestion that the nonrepetitive domain of the former is important in allowing the formation of a dense protein layer at the hydrophobic interface. Sequential adsorption studies showed that γ-gliadin could adsorb to a preexisting layer of ω-gliadin or could displace the ω-gliadin from the hydrophobic surface.
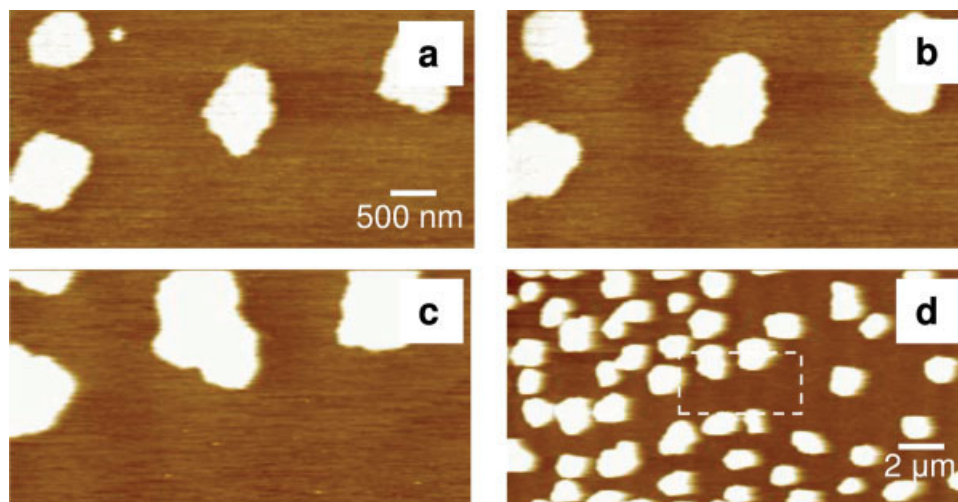
FIGURE 1 Demonstration of stability of gliadin adsorption to the interaction with the AFM probe. (a–c) sequence of 5 × 2.5 μm images of ω-gliadin structures on a mica substrate imaged in a 1% acetic acid environment; (d) subsequent 20 × 10 μm image showing no effect of the AFM probe in the original scan area.

However, ω-gliadin did not adsorb to a preformed layer of γ-gliadin when the reverse sequence was used.

A range of physical techniques have been used to elucidate features of protein adsorption on surfaces. These have included ellipsometry,[21] X-ray photoelectron spectroscopy,[22] AFM force measurements,[23] and quartz crystal microbalance.[24] However, the use of in situ AFM imaging to study the adsorption of the gliadin proteins should complement previous studies and provide new insights into the processes involved through the enormous advantage of providing real-time, nonspatially averaged visual data as the adsorption process unfolds.

MATERIALS AND METHODS

Protein Purification

Fractions containing γ-gliadins and "slow" ω-gliadins were purified essentially as described previously.[25] Milled grain (cv. Maris Butler) was stirred for 1 hr with 70% (v/v) aqueous ethanol at 20°C. After centrifugation, the supernatant was mixed with 1.5 M NaCl and left to stand at 4°C for 18 hr. The precipitated gliadin was removed by centrifugation, dissolved in 6 M urea and 0.01 M acetic acid, and separated into aggregates and monomers by gel filtration on a 90 × 4.4 cm column of Sephacryl S-300. Fractions containing monomers were bulked, dialyzed against water, and freeze dried. The monomer fraction was dissolved in 0.1 M acetic acid and separated by gel filtration on a 90 × 4.4 cm column of Biogel P-100. The γ- and ω-gliadins were separated by ion-exchange chromatography.

Atomic Force Microscopy

A Digital Instruments Multi-Mode AFM (Santa Barbara, CA) was used with a J-scanner (nominal 140 μm scan size) and 100-μm long oxide-sharpened silicon nitride cantilevers with a nominal spring constant of 0.38 N/m. The proprietary liquid cell was used without the silicon rubber O-ring inserted because surface tension forces were sufficient to constrain the liquid in the cell and therefore the O-ring was not required. Mica and HOPG substrates were obtained from Agar Scientific, UK, and Advanced Ceramics, CA, respectively.

After the freshly cleaved surface of the substrate had been imaged under 40 μL of the pure solvent (1% acetic acid), a 10-μL or 20-μL aliquot of protein solution in 1% acetic acid was injected into the liquid cell using a microsyringe. The injection process caused transient disruption to the image acquisition, but continuous imaging was achieved successfully, allowing the subsequent adsorption process to be followed from zero time. After the initial injection of protein, subsequent injections were sometimes made, allowing sequential processes, and the effects of changes in imaging environment to be observed. Figure 1 demonstrates that this method of imaging the adsorption process is not significantly affected by the action of the AFM probe on the substrate surface. In AFM images, the height of material above the substrate is indicated by a gray scale, with increasing brightness corresponding to increasing height. The bright areas on the images in Figure 1 correspond to patches of adsorbed protein, whereas the darker areas correspond to the substrate. Figures 1a–1c show a sequence of 5 × 2.5 μm scans of ω-gliadin structures on a mica substrate. On the subsequent scan, shown in Figure 1d, the scan size was increased to 20 × 10 μm, and it is observed that the original 5 × 2.5 μm image (area indicated by the dashed white rectangle) was typical of the surrounding area, which had not been near the AFM probe.

RESULTS AND DISCUSSION

Figures 2a–2f show a time course of the adsorption of ω-gliadin onto a hydrophilic mica surface from a 33 μg/mL solution in 1% acetic acid. In Figure 2, we see a process of nucleation and growth of ω-gliadin islands on the mica
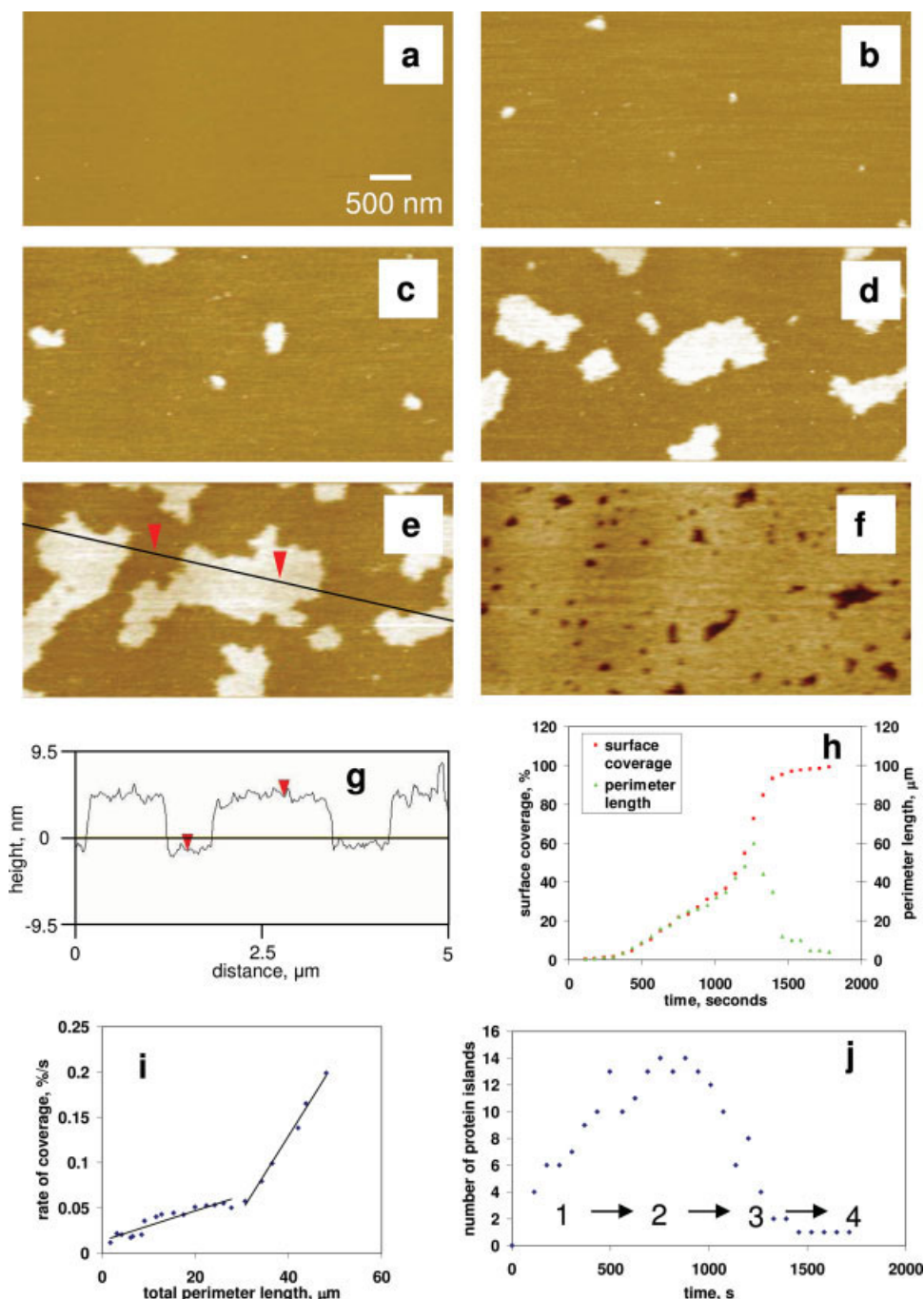
FIGURE 2 ω-Gliadin adsorption onto mica at pH 2.8. Sequence of images showing evolution of surface structures after addition of ω-gliadin solution to the buffer solution above freshly cleaved mica. (a) Mica imaged under 1% acetic acid; (b) 177 s after injection of protein; (c) 369 s after injection of protein; (d) 625 s after injection of protein; (e) 1009 s after injection of protein; and (f) 1457 s after injection of protein. The z-range is 0–20 nm. (h) Height profile along the diagonal line in e. (g) Graph of percentage surface coverage vs. time from the injection of protein onto the surface, and length of island perimeter (in the field of view) vs. time for the same period. (i) Graph of surface coverage rate vs. perimeter length. (j) Graph of number of islands visible in the field of view vs. time.

substrate. Growth and nucleation occur simultaneously, however, the adsorption occurs preferentially at the edges of preadsorbed structures, leading to rapid growth of the protein islands and a relatively low rate of formation of new nucleation sites. The protein islands grow until they contact each other, followed by slow infilling until the monolayer,
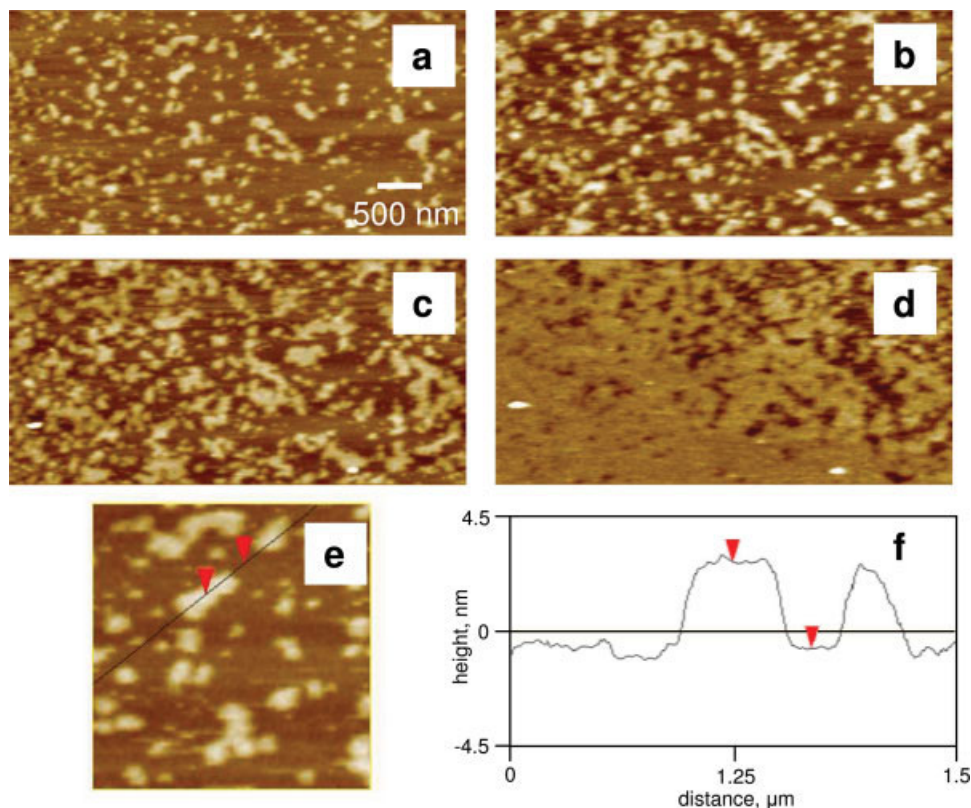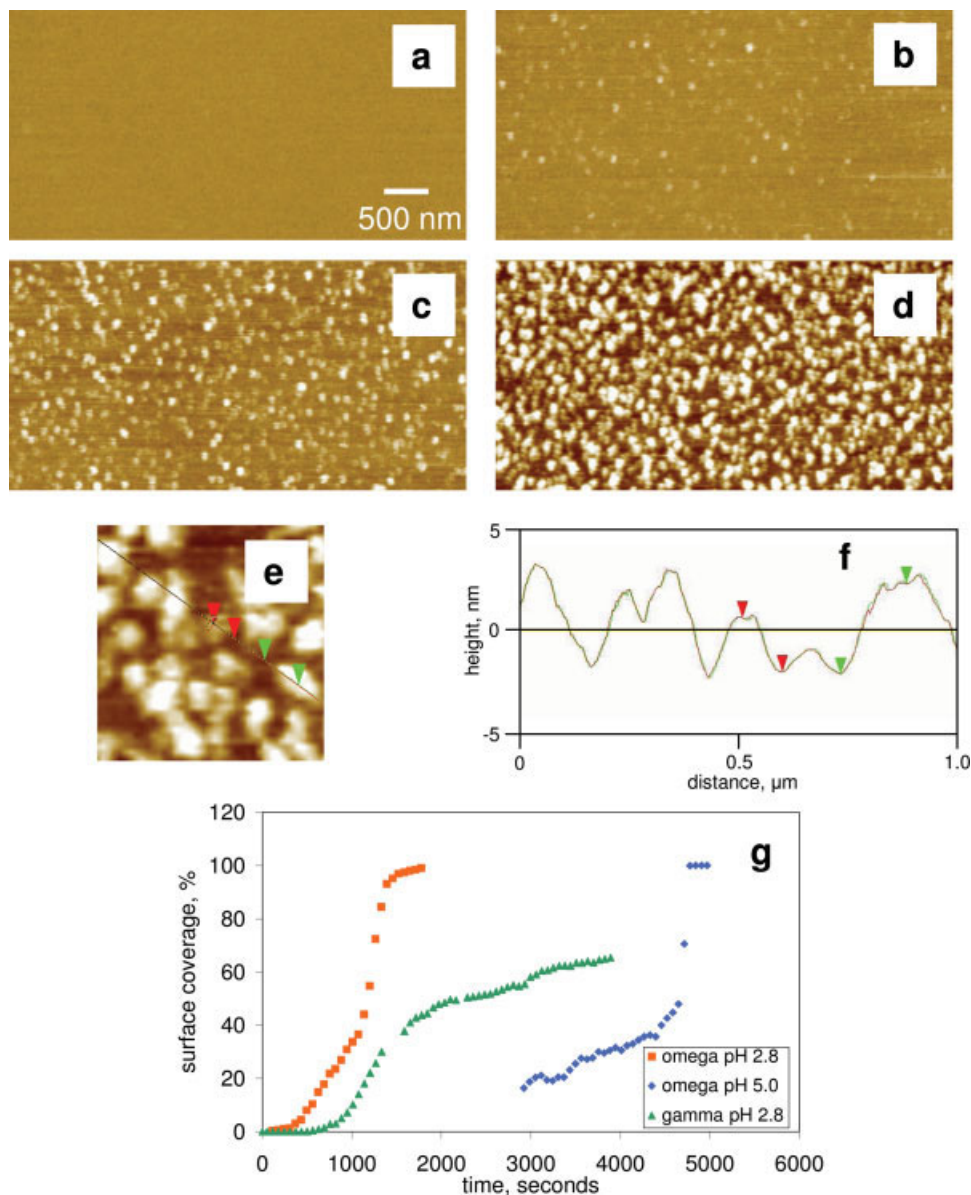
FIGURE 3 *ω*-Gliadin adsorption onto mica at pH 5.0. Sequence of images showing evolution of surface structures after addition of *ω*-gliadin solution to the buffer solution above freshly cleaved mica. (a) Three thousand two hundred twenty-four seconds after injection of protein; (b) 3627 s after injection of protein; (c) 4203 s after injection of protein; and (d) 4715 s after injection of protein. The z-range is 0–10 nm. (e) Zoomed area of image (a). (f) Height profile along the diagonal line in (e).

Figure 2h, is formed. Determination of the depth profile, Figure 2g, shows that adsorption does not occur on top of the existing protein islands. That no bi- or multilayer protein formation was observed in this experiment is consistent with the result of Örnebro et al.[11] who observed no significant increase in the amount of adsorbed *ω*-gliadin as the protein concentration was increased from 1 to 25 *μ*g/mL, although on a methylated silica surface. The height of the islands, 5 nm, is consistent with measurements of the diameter of the *ω*-gliadin molecule made by Thomson and coworkers[17] using STM and SAXS and therefore suggests that molecules adopt a side-on conformation to the mica surface (i.e., with the long axis parallel to the surface). It should be noted that 5 nm is greater than the diameter expected for a purely poly-L-proline II helical structure (∼1 nm); however; it is within the range expected for the diameter of a *β*-spiral consisting of poly-L-proline II and *β*-reverse turn (1.2–8 nm).[8] The results for *ω*-gliadin adsorption onto mica are consistent with the adsorption of the related protein C hordein onto mica, which also adsorbed in parallel to the surface and with apparent preference to the edges of preadsorbed structures.[6]

As mentioned above, the visual data of Figures 2a–2f show clearly that protein adsorption is favored at the edges of preadsorbed nucleation sites. This implies that the adsorption rate should be proportional to the perimeter length around the edges of growing and nucleating protein islands. Figure 2h shows, as a function of time, the percentage surface coverage of *ω*-gliadin and the total perimeter length measured around all the protein islands in the field of view. For times up to about 1200 s, Figure 2h seems to show proportionality with surface coverage. However, if the surface coverage is differentiated with respect to time and plotted against perimeter length, Figure 2i, we find two distinct regions of linear behavior. The rate of surface coverage increases slowly with perimeter length for low values and accelerates when the perimeter length exceeds about 30 *μ*m.

Figure 2j shows how the number of *ω*-gliadin protein islands in the field of view on the mica surface varied as a function of time. Interestingly, we can identify four regimes, broadly corresponding to times where the surface coverage graph changes slope. Regime 1, from 0 to ∼500 s, is predom-
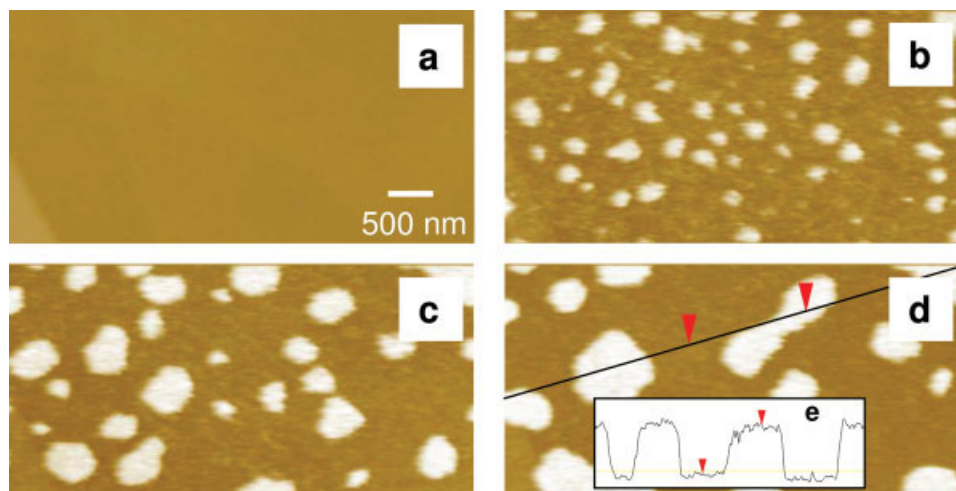
FIGURE 4 γ-Gliadin adsorption onto mica. Sequence of images showing evolution of surface structures after addition of γ-gliadin solution to the buffer solution above freshly cleaved mica. (a) Mica imaged under 1% acetic acid; (b) 920 s after injection of protein; (c) 1204 s after injection of protein; and (d) 2356 s after injection of protein. The z-range is 0–20 nm. (e) Inset zoom of image (d), and accompanying height profile (f). (g) Graph of percentage surface coverage.vs. time from the injection of protein, shown for γ-gliadin alongside both ω-gliadin at pH 2.8 and ω-gliadin at pH 5.0 for ease of comparison.

inantly characterized by nucleation of growth sites. Regime 2, from ~500 to ~1000 s, is characterized by growth of protein islands. In Regime 3, from ~1000 to ~1500 s, protein islands impinge and merge. Regime 4, from ~1500 s onwards, is characterized by infilling of holes in a single, continuous but 'holey', protein layer.

Considering Figures 2h and 2j together, along with the visual impression of nucleation and growth obtained from Figures 2a–2f, we can make some sense of the process involved. Starting from zero time, once a few nucleation sites have formed, there is an acceleration in surface coverage (at ~500 s) as islands begin to grow. There is a second acceleration in coverage at ~1000 s (~40% coverage), when islands begin to impinge. This corresponds to a maximization of adsorption sites as indicated by the nearby peak in total island perimeter length. After the protein islands start

FIGURE 5   *γ*-Gliadin adsorption onto graphite. Sequence of images showing evolution of surface structures after addition of *γ*-gliadin solution to the buffer solution above graphite. (a) Graphite imaged under 1% acetic acid; (b) 1676 s after injection of protein; (c) 1932 s after injection of protein; and (d) 2444 s after injection of protein. The z-range is 0–40 nm. (e) Height profile along the diagonal line in (d).

to significantly merge, the perimeter length and rate of surface coverage both become reduced. Finally, after ∼1500 s, there remains only slow infilling of holes in the protein layer.

Clearly, we have a complex adsorption dynamic because both the number and size of protein islands vary simultaneously through much of the process. Further, the concentration of protein in the solution would be decreasing as material adsorbed to the surface, although this effect is not considered significant because the initial quantity of protein in the solution is sufficient for the formation of ∼10–20 monolayers at 1–2 mg/m^2. The adsorption kinetics generally seem to be similar to a 2d Avrami process,[26] which has been used previously to describe the adsorption kinetics of poly-(*o*-methoxyaniline) in layer-by-layer films[27] and the adsorption from solution of hydrophobic–hydrophilic diblock copolymers to a hydrophilic silicon oxide substrate.[28]

In the previous experiment, shown in Figure 2, the pH of the 1% acetic acid imaging environment (∼2.8) is lower than the isoelectric point (pI) of the protein (6.4 < pH < 8.5), so the molecules will carry a net positive charge.[29] Furthermore, because the low pH will reduce, but not eliminate, the negative potential on the mica surface, it will continue to function as a negatively charged, hydrophilic surface so there will be an electrostatic attraction between the protein molecules and the mica substrate.[30,31] The effect of pH was investigated by an experiment involving the adsorption of *ω*-gliadin to a mica surface from solution at pH 5.0, which is thought to be the approximate vacuolar pH of the developing wheat grain.[32] This was achieved by the addition of KOH to the 1% acetic acid solvent before dissolution of the protein.

Figures 3a–d show a sequence of images illustrating the adsorption of *ω*-gliadin to mica from a solution of pH 5.0. At this pH, the adsorption is again parallel to the mica surface, as shown by the height of the adsorbed protein of ∼4 nm, Figures 3e and 3f. The isoelectric point of the mica surface is below 2, so increasing the pH from 2.8 to 5 will increase the surface density of negative charge.[33] However, the protein is now only slightly below its pI of 6.4–8.5, so its own net positive charge will be significantly lower than before. In contrast with the adsorption at pH 2.8, the *ω*-gliadin protein adsorbs randomly on the surface in these conditions, in a manner consistent with the random sequential adsorption model (RSA) and does not form the larger islands characteristic of pH 2.8.[34,35] This suggests that under these conditions protein–substrate interactions dominate over protein–protein interactions. Although the electrostatic repulsion between molecules will be reduced at pH 5, relative to pH 2.8, we must conclude that the increased negative charge density at the substrate compensates for any resultant increase in protein–protein interactions to an extent such that protein–substrate interactions dominate the adsorption process in this case.

The adsorption of *ω*-gliadin to mica at pH 5 takes significantly longer than at pH 2.8, Figure 4g. This indicates that the effect of increasing the pH is to weaken protein–substrate interactions, possibly through a reduced electrostatic attraction. As also observed in the experiment conducted at pH 2.8, there is a point of acceleration in the surface coverage vs. time plot for pH 5.0 adsorption, which in this case occurs at around 4600 s. As at pH 2.8, the rate of surface coverage at
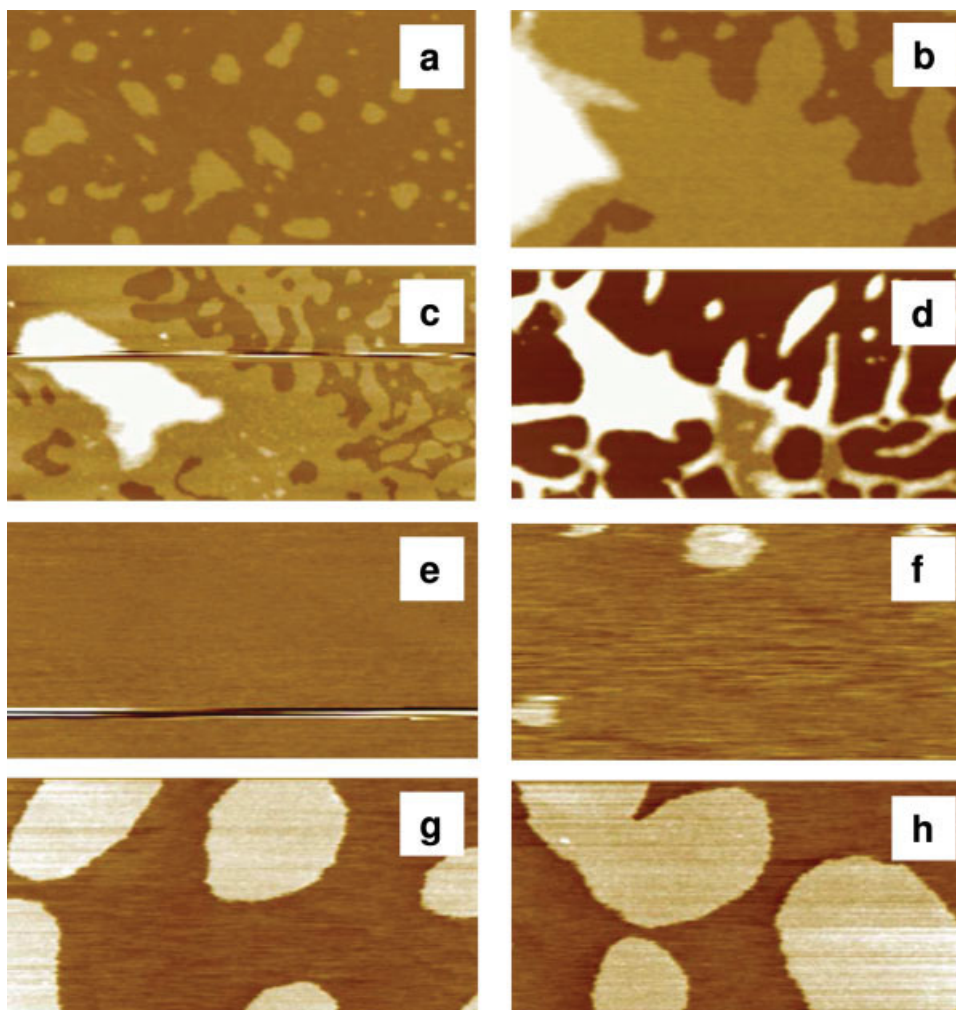
FIGURE 6 Sequential adsorption onto graphite: (a–d) γ-gliadin followed by ω-gliadin; (e–h) ω-gliadin followed by γ-gliadin. (a and b) $5 \times 2.5 \ \mu$m images 1869 s apart showing evolution of adsorbed gliadin structures; (c and d) $10 \times 5 \ \mu$m images: (c) injection of ω-gliadin and (d) the same surface 255 s after the injection of ω-gliadin. The z-range is 0–40 nm in (a–c) and 0–80 nm in (d). (e–h) $5 \times 2.5 \ \mu$m images, z-range is 0–20 nm. (e) Graphite imaged under 1% acetic acid with ω-gliadin present in the solution; injection of γ-gliadin near bottom of scan (f) 1257 s after injection of γ-gliadin; (g) 2660 s after injection; and (h) 3172 s after injection.

pH 5 increases at the point when coverage reaches $\sim$40%, suggesting that, as before, the number of available adsorption sites for ω-gliadin nears a maximum at this point.

Compared with the ω-gliadin adsorption at pH 2.8, the γ-gliadin protein adsorbs more slowly to mica at this pH, and presents as numerous randomly dispersed objects rather than discrete islands, Figures 4a–4d. Adsorption of the γ-gliadin to mica is presumably mediated via the "tail-like" hydrophilic N-terminal domain of the protein. The effect of surface properties on conformation of human plasma fibronectin was observed by AFM by Bergkvist et al.,[36] who noted that the fibronectin molecule was predominantly compact on hydrophilic silica, compared with a more compact structure

on hydrophobic methylated surfaces. We do not observe a surface-mediated denaturing effect on the γ-gliadin protein, possibly due to the presence of the intramolecular disulphide bonds stabilizing the structure.

The height profile of the isolated structures, Figures 4e and 4f, shows a bimodal distribution at 3 and 6 nm. These values compare well with those reported by Thomson et al, for the respective dimensions of the hydrophilic "tail-like" N-terminal domain and the hydrophobic "globular" C-terminal domain of γ-gliadin.[19] There may also be some tilting of the structures with respect to the surface, as speculated by Örnebro et al.[12] Comparing the adsorption of the two proteins onto mica after approximately equal times, Figure 4 g,
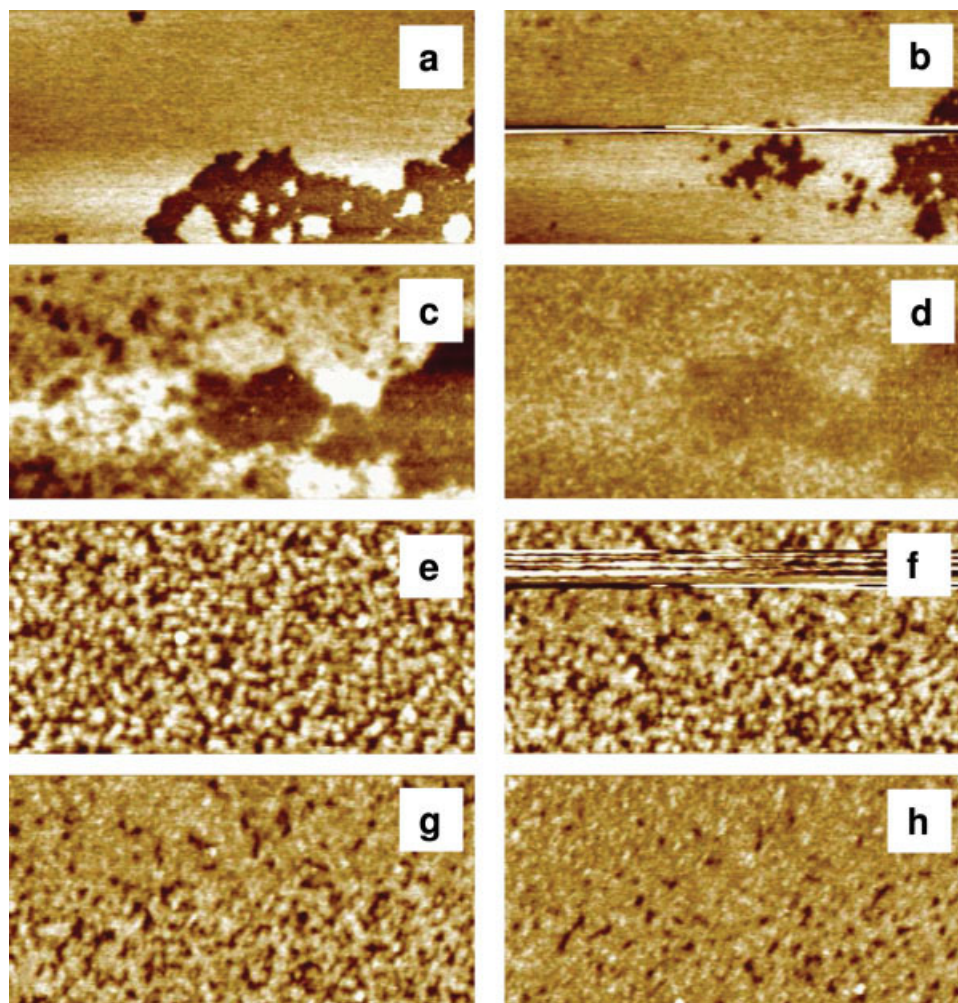
FIGURE 7   Sequential adsorption onto mica: (a–d) ω-gliadin followed by γ-gliadin; (e–h) γ -gliadin followed by ω-gliadin. (a) partial ω-gliadin monolayer; (b) injection of 10 μL γ-gliadin solution (c) 193 s after injection; (d) 705 s after injection. (e) γ-gliadin structure 3840 s after injection; (f) injection of 10 μL of ω-gliadin solution; (g) 768 s after injection; (h) 1535 s after injection. All images are 5 $\times$ 2.5 μm; (a–d) z-range is 0–20 nm; (e–h) z-range is 0–10 nm.

shows that the surface coverage is significantly lower for the γ-gliadin, which may relate to its more hydrophobic nature. The more compact structure of the γ-gliadins could lessen the mobility and rearrangement of the molecules on the surface, whereas the lack of association of the molecules may imply that the binding to the mica restricts the ability of the molecules to form intermolecular hydrogen bonds.

The adsorption of the γ-gliadin onto hydrophobic graphite occurs more slowly than the adsorption onto mica, Figures 5a–5d, which is most likely due to the absence of an electrostatic attraction between the protein and substrate in this case. The adsorption of γ-gliadin to graphite is unambiguously end-on (i.e., with long axis perpendicular to the surface) with mobile islands of height 12 nm, Figure 5e. Pre-

sumably, adsorption to the surface is via the hydrophobic C-terminal domain in this case, which would leave the hydrophilic N-terminal domain exposed to the solvent. Qualitatively, the adsorption is similar to that of the ω-gliadin onto mica. The end-on adsorption would also seem to encourage the side-to-side association between adjacent molecules, probably involving hydrogen bonds.

The behavior of the ω-gliadin on this hydrophobic graphite surface was markedly different: no stable adsorption of protein structures was observed in this case. This is in surprising contrast to the behavior of the related C hordein protein, which adsorbed more readily to hydrophobic graphite than to hydrophilic mica.[6] However, our result is more consistent with the expected hydrophilic nature of the rod-like ω-gliadin molecule.

The comparative interfacial properties of the two proteins are illustrated by sequential adsorption experiments. In Figure 6, γ-gliadin was first allowed to adsorb onto graphite, and then an aliquot of ω-gliadin solution was added to the liquid environment. After the initial growth of islands as seen in Figure 5, the addition of the ω-gliadin seemed to lead to a 'dewetting' of the surface, Figure 6d. By this we mean that the surface-adsorbed γ-gliadin contracts away from the graphite surface into the observed high ridges of material. Figures 6a–6c have height scales of 0–40 nm, whereas Figure 6d has a height scale of 0–80 nm. The height of the surface-adsorbed protein above the substrate is indicated in the images by the relative brightness, so there is clearly a significant increase in height between Figures 6c and 6d. This observation is at first sight contradictory with that of Örnebro et al.,[11] who saw no change in surface coverage on adding ω-gliadin to preadsorbed γ-gliadin, although it should be noted that Örnebro et al. used a hydrophobic methylated silica surface as opposed to the graphite surface used here. Another possibility is that the dewetting of the surface, with consequent local increases in height of the aggregated material, Figure 6d, has not altered the amount of protein on the surface, but merely the local concentration and coverage. This dewetting effect would imply that association between ω- and γ-gliadins is stronger than the adsorption of the γ-gliadin to the surface. A possible explanation is the interaction between the hydrophilic ω-gliadins in solution and the exposed hydrophilic N-terminal domains of adsorbed γ-gliadin molecules. In a parallel experiment, shown in Figures 6e–h, an ω-gliadin solution was presented to a hydrophobic graphite surface. As would be expected from previous results, stable adsorption was not observed. Injection of an aliquot of γ-gliadin solution led to the progressive development of surface-adsorbed islands similar to that seen on graphite with only γ-gliadin present (Figure 5). Kinetically and structurally, the γ-gliadin behaves largely as if the ω-gliadin is not present. This confirms the more hydrophobic behavior of the γ-gliadin.

The sequential adsorption behavior on mica is illustrated in Figure 7. On the addition of γ-gliadin to an adsorbed ω-gliadin monolayer, Figure 7b, the almost complete monolayer begins to develop pits, indicated by the rougher looking and less regular surface of the protein layer, and there is a loss of material from around the edges. The physical asymmetry of the γ-gliadin molecule, in comparison with the rod-like ω-gliadin, may lead to disruption of the very regular packing of the latter on mica. In contrast, starting with a hydrophobic surface, Örnebro et al.[11] observed an increase in surface coverage when γ-gliadin was added to ω-gliadin. In competitive adsorption studies involving BSA and collagen

molecules, it was observed that, although dissimilar in shape and aspect ratio, the surface affinity was the main controlling factor.[21]

The reverse process, in which ω-gliadin was added to an adsorbed γ-gliadin surface, is shown in Figures 7e–7h. This is more difficult to interpret because of the less regular structure of the γ-gliadin deposits on the hydrophilic mica. However, there does seem to be a gradual infilling of the "holey" γ-gliadin surface, resulting in an uneven bumpy surface, Figure 7h. This irregular surface most probably results from the different conformations of the two proteins on the mica, with a low amount of available binding sites for the ω-gliadin molecules favoring a side-on mode of adsorption.

CONCLUSIONS

The direct imaging capability of AFM has revealed significant differences between the surface adsorption behavior of the ω- and γ-gliadin proteins on two model surfaces: hydrophilic mica and hydrophobic graphite. In situ real-time imaging of molecular adsorption to a substrate allows analysis of the dynamics of molecular attachment and its modulation by the character of the substrate. The more hydrophobic behavior of the γ-gliadin compared with the ω- gliadin was confirmed by the ability of the former to form near-monolayers on graphite; the opposite behavior was observed on mica. Both proteins adsorbed to mica, but the ω-gliadin adsorption was more regular and more rapid. The γ-gliadin showed ordered adsorption onto graphite in an end-on orientation, implying the existence of well-defined and distinct hydrophobic and hydrophilic "patches" on the surface of the molecule. The sequential pairwise adsorption behavior was not commutative. On mica, the γ-gliadin seemed to partly displace the preadsorbed ω-gliadin, while reversing the order produced an infilling of the noncontinuous γ-gliadin layer. On graphite, the most striking result was the dewetting of the γ-gliadin surface layer by the addition of the ω-gliadin solution, most likely caused by some γ–ω interaction, destabilizing the γ-gliadin interaction with the surface. Future investigations could involve using the AFM to directly measure gliadin–gliadin and gliadin–substrate interaction forces (in a manner similar to Paananen et al.[13]), which would provide valuable complimentary information to the present study.

REFERENCES

1. Drake, B.; Prater, C. B.; Weisenhorn, A. L.; Gould, S. A. C.; Albrecht, T. R.; Quate, C. F.; Cannell, D. S.; Hansma, H. G.; Hansma, P. K. Science 1989, 243, 1586–1589.

2. McMaster, T. J.; Miles, M. J.; Kasarda, D. D.; Shewry, P. R.; Tatham, A. S. J Cereal Sci 1999, 31, 281–286.

3. Lin, J. N.; Drake, B.; Lea, A. S.; Hansma, P. K.; Andrade, J. D. Langmuir 1990, 6, 509–511.

4. Stipp, S. L. S. Langmuir 1996, 12, 1884–1891.

5. Ta, T. C.; Sykes, M. T.; McDermott, M. T. Langmuir 1998, 14, 2435–2443.

6. McMaster, T. J.; Miles, M. J.; Shewry, P. R.; Tatham, A. S. Langmuir 2000, 16, 1463–1468.

7. Shewry, P. R.; Miles, M. J.; Tatham, A. S. Prog Biophys Mol Biol 1994, 61, 37–59.

8. McIntire, T. M.; Lew, E. J. L.; Adalsteins, A. E.; Blechl, A.; Anderson, O. D.; Brant, D. A.; Kasarda, D. D. Biopolymers 2005, 78, 53–61.

9. Kim, D. T.; Blanch, H. W.; Radke, C. J. Langmuir 2002, 18, 5841–5850.

10. Shewry, P. R.; Popineau, Y.; Lafiandra, D.; Belton, P. Trends Food Sci Technol 2001, 11, 433–441.

11. Örnebro, J.; Wahlgren, M.; Eliasson, A.-C.; Fido, R. J.; Tatham, A. S. J Cereal Sci 1999, 30, 105–114.

12. Örnebro, J.; Nylander, T.; Eliasson, A.-C. J Cereal Sci 2000, 31, 195–221.

13. Paananen, A.; Tappura, K.; Tatham, A. S.; Fido, R.; Shewry, P. R.; Miles, M.; McMaster, T. J. Biopolymers 2006, 83, 658–667.

14. Tatham, A. S.; Shewry, P. R. J Cereal Sci 1995, 22, 1–16.

15. Tatham, A. S.; Drake, A. F.; Shewry, P. R. Biochem J 1989, 259, 471–476.

16. Wellner, N.; Belton, P. S.; Tatham, A. S. Biochem J 1996, 319, 741–747.

17. Shewry, P. R.; Miles, M. J.; Thomson, N. H.; Tatham, A. S. Cereal Chem 1997, 74, 193–199.

18. Tatham, A. S.; Masson, P.; Popineau, Y. J. Cereal Sci 1990, 11, 1–13.

19. Thomson, N. H.; Miles, M. J.; Tatham, A. S.; Shewry, P. R. Ultramicroscopy 1992, 42, 1204–1213.

20. Bietz, J. A.; Burnouf, T. Theor Appl Genet 1985, 70, 599–609.

21. Ying, P.; Yu, Y.; Jin, G.; Tao, Z. Colloids Surf B: Biointerfaces 2003, 32, 1–10.

22. Browne, M. M.; Lubarsky, G. V.; Davidson, M. R.; Bradley, R. H. Surf Sci 2004, 553, 155–167.

23. Dupont-Gillian, Ch. C.; Fauroux, C. M. J.; Gardner, D. C. J.; Leggett, G. J. J Biomed Mater Res 2003, 67, 548–558.

24. Choi, K. H.; Friedt, J. M.; Laureyn, W.; Frederix, F.; Campitelli, A.; Borghs, G. J Vac Sci B 2003, 21, 1433–1436.

25. Tatham, A. S.; Shewry, P. R. J Cereal Sci 1985, 3, 103–113.

26. Avrami, M. J Chem Phys 1939, 7, 1103–1112.

27. Raposo, M.; Oliveira, O. N. Langmuir 2002, 18, 6866–6874.

28. Abraham, T.; Giasson, S.; Gohy, J. F.; Jerome, R.; Muller, B.; Stamm, M. Macromolecules 2000, 6051–6059.

29. Sodergaard, I.; Jensen, K.; Krath, B. N. Electrophoresis 1994, 15, 584–588.

30. Scales, P. J.; Grieser, F.; Healy, T. W. Langmuir 1990, 6, 582–589.

31. Raiteri, R.; Martinoia, S.; Grattarola, M. Biosens Bioelectron 1996, 11, 1009–1017.

32. Miller, A. J.; Cookson, S. J.; Smith, S. J.; Wells, D. M. J Exp Bot 2001, 52, 541–549.

33. Nishimura, S.; Tateyama, H.; Tsunematu, K.; Jinnai, K. J Coll Int Sci 1992, 152, 359–367.

34. Talbot, J.; Tarjus, G.; Van Tassel, P. R.; Viot, P. Colloids Surf A 2000, 165, 287–324.

35. Almeida, A. T.; Salvadori, M. C.; Petri, D. F. S. Langmuir 2002, 18, 6914–6920.

36. Bergkvist, M.; Carlsson, J.; Oscarsson, S. J Biomed Mater Res A 2002, 64, 349–356.

Reviewing Editor: Nils G. Walter